Effective anti-biofouling enabled by surface electric disturbance from water wave-driven nanogenerator

Yin Long[1,2], **Yanhao Yu**[1], **Xin Yin**[1], **Jun Li**[1], **Xiaosong Du**[2], **Yadong Jiang**[2], and **Xudong Wang**[1]

[1]Department of Materials Science and Engineering, University of Wisconsin-Madison, Madison, Wisconsin 53706, United States

[2]State Key Laboratory of Electronic Thin Films and Integrated Devices, School of Optoelectronic Information, University of Electronic Science and Technology of China, Chengdu, 610054, China

Abstract

Biofouling has been a long-last problem in a variety of marine systems which causes energy waste and device damage. In this study, we present a self-activated anti-biofouling system enabled by electrical double layer disturbance, which could effectively suppress the initial formation of conditioning layers and subsequent microbe attachment. The small and low-frequency alternating electrical fields were produced by a triboelectric nanogenerator under water wave impacts. Systematic analyses confirmed that the anti-biofouling efficacy was directly related to the strength of the electric field and was effective in both fresh lake and sea water environments. An on-site demonstration was implemented at a calm lake shore for three weeks. The water wave-driven anti-biofouling exhibited excellent surface protection, which was significantly superior to several commercial anti-biofouling coatings. This development brings a novel, effective and eco-friendly solution for protecting a broad range of surfaces against biofouling.

Keywords

Anti-biofouling; Electric double layer; Surface conditioning film; Self-activation; Nanogenerator

1. Introduction

The attachment and accumulation of organic substances and subsequent microbe attaching on submerged solid surfaces (*e.g.*, ship's hulls, underwater pipes, oceanographic sensors, drilling equipment, oil platforms, fishing nets, power plants and aquaculture systems), can cause substantial energy waste and severe damage through increasing fuel consumption, blocking pipes, accelerating metal corrosion, boosting engine stress and destroying underwater instrument.[1–7] It is known that biofouling begins with the formation of a molecular surface "conditioning" layer, which contains organic substances (*i.e.* proteins, glycans, humic acids, carbohydrates, and/or unspecified macromolecules etc.) and works as linking layer for further microbes growth settlement and nutrition supplies.[8–12] 8 Nowadays,

xudong.wang@wisc.edu (XW).

prevailing anti-biofouling strategies are focusing on novel coating materials[13–19] and developing effective electrochemical sterilization procedures[20–22]. For example, nanostructured materials with super-hydrophobic self-cleaning surfaces, and hyper-branched polymer structures with hydrophilic-ended or activated foulant releasing groups are incorporated in most current coating techniques. However, advanced coatings usually associated with reduced mechanical properties (*e.g.* more vulnerable to cutting, tearing or puncturing and weaker adhesion to substrate), sophisticated fabrication processes, and extensive use of chemicals resulting in higher costs and more environmental issues.[23, 24] On the other hand, electrochemical sterilization typically relies on locally generating biocides (e.g. reactive oxygen species) *via* electrochemical water electrolysis or by immobilizing electro-generated biocides. This strategy, however, imposes high and selective requirements on surrounding environments for biocides generation and interaction. Additionally, electric fields have also been investigated as a promising anti-biofouling strategy. Conventional electrical anti-biofouling techniques typically use an alternative strong electric field (1–100 kV/cm) with a high-frequency (up to 1000 Hz) to kill microbes by irreversible electroporation of cell membranes[25] or to repel microbes via the dielectrophoresis effect.[26] These electrical anti-biofouling techniques are generally very effective but are usually used in small systems (e.g. biomedical devices) due to the complexity of electrical setup.

Recently, nanogenerator (NG) was developed as an effective approach to converting environmental mechanical energy into electricity.[27–32] With appropriate design, the electric potential generated directly from water agitation can be utilized as a self-sustainable energy source to achieve active anti-biofouling. Pioneer research has shown that high electric potential (a few hundred volts) from water-driven triboelectric nanogenerators (TENGs)could effectively prevent microbes adhesion on the electrode covered area by applying pulsed positive and negative potential to anode and cathode, respectively, so as to change surface charge distribution on microbes to prevent their adhesion.[33] This work demonstrated the feasibility of self-activated anti-biofouling strategy by direct mechanical energy conversion. However, the requirement of high electrical field and full electrode coverage to achieve anti-biofouling brought a high demand on electrode design and system integration, which may become a practical issue in large scale applications. In this work, we demonstrated a self-activated anti-biofouling strategy by introducing a low frequency and low intensity alternative electric field between a pair of wire electrodes using a water wave-driven TENG. In this design, the biofouling was effectively restricted by suppressing the evolution of the conditioning film in the initial stage through disturbing the electrical double layer in between the two electrode wires. A long-term test in fresh water evidenced that small lake shore waves achieved significantly more effective anti-biofouling results compared to commercial anti-biofouling coatings.

2. Experimental Section

2.1 Fabrication and characterization of Triboelectric Nanogenerators (TENG).

(A) Contact-mode TENG: A kapton film (7.5 cm × 2.5 cm) was attached to an ITO/PET substrate of the same size, which was considered as the top electrode. Bottom electrode was a piece of Cu foil (7.5 cm × 2.5 cm) on a glass substrate (7.5 cm × 2.5 cm). These two

electrodes were separated by two pieces of glass spacers (1 mm in thickness) and connected to the external circuit through Al leads. During the measurement, the top electrode was pressed to the bottom electrode by a computer controlled actuator with a frequency of 5 Hz and the bottom electrode was anchored on the table surface. The voltage outputs were recorded by an Agilent DSO1012A oscilloscope. The current outputs and charge transfer were measured by an Autolab PGSTAT302N station.

(B) Water-driven TENG: A kapton film (5 cm × 2.5 cm) was attached to an ITO/PET substrate (5 cm × 2.5 cm) as the top electrode. Bottom electrode was a piece of Cu foil (5 cm × 2.5 cm) on a glass substrate (7.5 cm × 2.5 cm). These two electrodes were separated by thermally bending the top electrode into an arch shape, where the separation distance at the middle of the arch was 5 mm. Al leads encapsulated by epoxy was used to connect the two electrodes and fixed onto the exposed glass surface. The TENG part was sealed in by a plastic film and epoxy. The water-driven TENG was fixed on a wood panel together with aluminum and copper foil, and then half immersed into Lake Mendota, Madison, WI for 3 weeks.

2.2 Selection and Enrichment of Natural Lake and Sea Water Bath.

Fresh natural lake water was collected from Lake Mendota, Madison, WI. The fresh water was stored in a refrigerator at 4 ℃ for no more than 3 day uses. 10 mg NaHPO$_4$, 10 mg KNO$_3$, 10 mg CaCO$_3$, 10 mg MgSO$_4$, 2 mg FeSO$_4$ and 1 g potato dextrose were added into 50 ml DI water, stirred for 24 h and autoclaved for 1 h to form a homogenous nutrient solution. 20 ml of this nutrient solution was added into 30 ml of the fresh natural lake water for biofouling test. Sea water was collected from Carson Beach, Day Boulevard, South Boston, MA. The sea water was utilized immediately after overnight delivery. 1 g potato dextrose were added into 50 ml synthetic sea water (CarolinaBiologicalSupplyCompany), stirred for 24 h and autoclaved for 1 h to form a homogenous nutrient solution. 20 ml of this nutrient solution was added into 30 ml of the natural sea water for biofouling test.

2.3 Commercial Antifouling Coating Comparison.

Four mainstream commercial antifouling coatings are selected to conduct control experiments for efficacy comparison. The coatings included hard hybrid ablative antifouling paint (KOP-COAT. Inc.), aerosol antifouling paint (KOP-COAT. Inc.), marine grade Aquagard paint (Flexdel Corp.) and Aluminipaint (TotalBoat corp.). Each commercial coating was applied to an equal area (3 cm × 3 cm) on the same wooden test panel with their edges sealed by epoxy. A self-activated antifouling system was also mounted next to the painted area. The wood panel was half immersed into Lake Mendota, Madison, WI for 4 weeks, and all the painted surfaces were completely immersed below the water surface.

2.4 Adsorption Tests.

The adsorption test of potato dextrose onto a glass surface was performed at 25 °C under ambient conditions as follows. A glass slide was cleaned with ethanol, acetone, and DI water for 15 min under ultrasonic bath successively, and was placed into a 50 ml pre-made potato dextrose solution (1g/50 ml) for 2 h. Then the glass slide was taken out from the solution

and rinsed three times with DI water to remove loosely absorbed substances. The substrate was then dried under vacuum for further characterization.

2.5 Morphology and Elemental Characterizations.

Microscopy images were obtained with a CCD camera (Olympus, Japan) mounted on an upright microscope (Axio Imager A2, Zeiss), and recorded through Image J software. XPS was conducted on a Thermo Scientific K-alpha XPS instrument. The survey range was from 0 to 1000 eV. The C 2p, O 2p, N 2p spectra were highlighted for characterizing the possible absorbed organic substance on the surface of the glass substrate. AFM images were obtained by a XE-70 Park system.

3. Results and Discussions

The self-activated anti-biofouling was first implemented using a simple contact-mode TENG to provide electrical field driven by a computer-controlled actuator. As shown in Figure 1A, the TENG device was directly connected to two aluminum leads, which were fixed on a glass substrate and encapsulated by ~ 0.2 mm epoxy. These two leads were placed 0.5 cm apart from each other, separating the substrate into protected area (area between two wires) and unprotected area (area outside of the two wires). The glass substrate was immersed into natural lake water, which was enriched with potato dextrose (a general microbiological growth nutrient) to accelerate microbe growth and adhesion. Alternating electrical potential generated by the TENG was remained at a steady ±6 V at a frequency of 5 Hz (Figure 1B). This voltage corresponded to ±12 V/cm electric field in between the electrode. The asymmetric voltage output was a result of the relatively low internal resistance (~1 MΩ) of the oscilloscope. Corresponding short-circuit current (I_{sc}) and voltage outputs at 0.5–4 Hz agitations were included in the Supporting Information (Figure S1). After 16-hour operation, the glass substrate was removed from the water bath and the surface was observed by an optical microscope. The control surface (bare glass substrate) exhibited a dense layer of microbes with various types and dimensions (Figure 1C). The unprotected area on the testing glass substrate showed a similar microbes coverage as the control surface (Figure 1D). At the spot where the electrode wire was placed, there exited a sharp boundary clearly showing the drastic difference in microbe adhesion between protected and unprotected areas (Figure 1E). In contrast to unprotected area, very little adhesion was observed in the protected area between the two electrodes (Figure 1F).

Considering the major antifouling strategies are practiced in the ocean, the same set of experiment was carried out in sea water (obtained from the Carson Beach, Day Boulevard, South Boston, MA, USA). After 16 hours emerged in the sea water enriched with potato dextrose, the protected glass substrate also exhibited similar strong contrast in microbe adhesion between protected area (Figure S2B) and unprotected area (Figure S2C). An apparent boundary (Figure S2A) was also observed at the position where the electrode wires were placed (Figure S2A and C). These initial observations explicitly proved the excellent performance of this anti-biofouling strategy in both fresh and sea water.

The anti-biofouling enabled by the discrete, low amplitude and alternating electric fields could be attributed to the electric field-induced disturbance to the electrical double layer,

which impairs the formation of the conditioning layer in the initial biofouling stage. As schematically shown in Figure 2A, when a substance is placed in a natural water electrolyte, an electrical double layer will form at the surface, which provides electrostatic force to attract organic substances toward the surface[34]. Supported by the organic substances, small microbes, such as bacteria and diatoms can gather and attach to the solid surface. Hereto the process is reversible and both organic substances and small microbes can be easily removed by fluid shear forces. Stable and irreversible attachment occurs when the microbes secrete extracellular polymer substances (EPS), creating a hydrated, heterogeneous and slimy matrix that holds the microbes together and binds the microbes tightly to the substrate surface[35–37]. Presence of a weak and low-frequency alternating electric field, although can't generate a strong electrophoresis force to push away the microbes as the well-practiced electrical anti-biofouling process, can instead influence the stable distribution of the electrical double layer. As shown in the bottom panels of Figure 2A, the ion distribution in the double layer fluctuates as the electric field oscillates back and forth. Thus, the electrostatic force for attracting organic substances becomes unstable, and the gathering of microbes is interrupted. Without a steady position, the microbes were unable to generate sufficient EPS to initiate irreversible attachment. Therefore, biofouling is suppressed.

This mechanism was first validated by testing the nutrient (potato dextrose) adsorption in a microbe-free water environment. The same anti-biofouling glass slide was immersed in deionized (DI) water with 1 g/50 ml of potato dextrose for 1 hour. Atomic force microscopy (AFM) topological scans showed that the surface roughness of unprotected area was 200 nm (Figure 2B); whereas the protected area only had a surface roughness of 80 nm (Figure 2C), suggesting significantly more substances were adsorbed on the unprotected area. X-ray photoelectron spectroscopy (XPS) analysis revealed that the nanoscale attachment contained rich amount of C, O, and N elements. While both C and O elements could also be observed from the protected area (Figure S3), no N characteristic peaks could be identified from the protected area (Figure 3D). The deconvoluted N 2p peak at 400 eV corresponds to the C-NH_2 bonds, while the 401.5 eV peak is from the protonated N element of amino group[38], confirming the attached substances were potato dextrose nutrient. The new N 2p peak at 402.6 eV could be attributed to the N-Si-O bond, suggesting a stable absorption of the organic substance in the unprotected area[39].

To directly evidence the disturbance on electrical double layer by the weak electric field, we introduced an additional "reference" electrode in the middle between the two working electrodes. As schematically shown in Figure 2E, the two working electrodes were electrically isolated from solution and connected to a TENG to generate a desired electric field. The reference electrode was directly grounded and the current flow between the reference electrode and ground (I_R) was monitored. At equilibrium, no charge flow would be detected. However, when the ion concentration in the double layer varied, to balance the surface charge, a surge of charge flow could be induced between the ground and the reference electrode (I_R 0). The direction of I_R was determined by the ionic charge and relative concentration change. Figure 2F (complete current output curve is shown in Figure S4) illustrates the I_R change when the TENG was activated. Although there was no current flow between the two working electrodes, sharp current peaks were recorded from the

reference electrodes, confirming ion concentration fluctuation in the double layer upon the appearance of a small transient electric field.

To further investigate the anti-biofouling efficacy controlled by the electrical double layer disturbance, the microbe attachment was statistically analyzed under variable circumstances. First, the electric field influences were studied by changing the electrode distances from 0.5 cm to 1.5 cm. All the electrode spacing (0.5 cm, 0.8 cm, 1.0 cm, 1.2 cm, 1.5 cm) exhibited appreciable anti-biofouling phenomenon and all the protected and unprotected areas could be clearly identified (Figure S5). While all the unprotected areas showed a very similar high density microbe coating, the appearance of microbes in the protected areas became more obvious when the electrode spacing was above 1.0 cm. To obtain a more quantitative understanding, the average numbers of microbes along the horizontal position (Figure 3A) 10 mm below water surface were collected from the first three smaller electrode spacing samples. The numbers were counted from 15 optical images randomly taken from a 65×65 μm^2 area, and plotted as a function of the horizontal position (Figure 3B), the center between the two electrodes was defined as 0). As expected, all the unprotected areas had the same microbe density (3.5×104 mm^{-2}), and this value was sharply reduced by at least 85% in the protected areas. This anti-biofouling efficiency is generally superior as compared to those most current representative anti-biofouling technologies, as detailed in Table S1. Specifically, the 0.5 cm electrode pair showed the lowest microbe density (375 mm^{-2}) and the distribution was fairly uniform across the entire 0.5 cm region. The microbe density rose to 1000 mm^{-2} and 1100 mm^{-2} as the electrode spacing increased to 0.8 cm and 1.0 cm, respectively. Meanwhile, the attachment distribution became less uniform with the lowest density being at the center point (x=0). This could be attributed to stronger fluid shear force at the center areas. The microbe density at x=0 were plotted as a function of the electrode spacing as well as the electric field (Figure 3C). A linear relationship with a slope of 40.3 could be extrapolated between the microbe density and the electric field strength, *i.e.* the less electric field strength between the electrodes, the more microbes were attached to the glass substrate.

For anti-biofouling application, the entire surface underneath the water needs to be protected. Therefore, it is also important to confirm how deep the anti-biofouling would remain effective. In principle, since the electrode wires were electrically isolated from the water electrolyte, the electric potential would be independent to the length of wire. Thus, the anti-biofouling efficacy should remain unchanged regardless how deep the electrode wires were extended under the water surface. This hypothesis was tested in a lab-scale small system, where the underwater section of the insulated electrode wires was adjusted to >2 cm. After 16-hour operation, the microbe densities at the center point were quantified along the vertical direction (*i.e.* depth) for 0.5, 0.8 and 1.0 cm electrode spacing and plotted in Figure 3D. The 0.5 cm spacing sample exhibited a fairly flat density distribution, suggesting the anti-biofouling was indeed independent to the depth of water within the testing regime. Nevertheless, the 0.8 cm and 1.0 cm spacing samples showed a very subtle increase in microbe attachment (<10%). This was possibly due to small charge leakage and surface screening effect at large electrode lengths, which became more sensitive at lower electric fields when the electrode spacing was large.

In addition, the frequency dependence was investigated by varying the mechanical impact frequency from 0.5 Hz to 5 Hz. As shown in Figure 3E, higher densities of microbe attachment were observed at lower frequencies, suggesting the anti-biofouling would be more effective when the electric field was switched faster, *i.e.* more intense disturbance to the double layer. For both lower electric field cases (*i.e.* 0.8 cm and 1.0 cm electrode spacing), this relationship was almost linear within the testing frequency range. However, for the higher electric filed case (0.5 cm electrode spacing), although the overall microbe density was lower than the other two cases due to the higher electric field, the anti-biofouling efficacy exhibited a tendency to reach a saturated value as the frequency increased to above 3 Hz.

After obtaining necessary fundamental understandings in a lab-scale simulated system, an on-site demonstration was development. Figure 4A shows the schematic structure of a water wave-driven anti-biofouling system. An arch-shaped contact mode TENG was fabricated to cover the top ~2/3 surface area of a glass slide. Two epoxy-encapsulated Al wires were connected to the two TENG electrodes and affixed to the bottom portion of the glass slide. The actual device is shown in Figure 4B. Under normal wave impacts, the electric potential generated in between these two Al wires were measured to be in the range of ~1–3 V (Figure 4C), corresponding to an electric field of 2–6 V/cm. Together with a series of control surfaces (including aluminum and copper foil), this device was placed at the shore of Lake Mendota for 3 weeks (Inset of Figure 4A). As shown in Figure 4D, the protected area between the two Al wires was obviously clean in strong contrast to the unprotected areas, which were obviously fouled. A sharp boundary could be observed under optical microscope (Figure 4E). For comparison, the Cu and Al foil surfaces also exhibited significant biofouling phenomenon under the same condition (Figure 4F and Figure S6), although copper is still the prevailing component in current anti-biofouling coatings. This experiment clearly evidenced that small water waves in a calm lake can effectively protect the surface from biofouling in our system.

The effectiveness of this antifouling strategy was further evaluated by comparing to four commercial antifouling coatings, *i.e.* Hard hybrid ablative antifouling, Aerosol antifouling paint, Marine grade aquagard paint, and Aluminipaint (Figure 4G and Figure S7). After four weeks of on-site test in Lake Mendota, all commercial coatings exhibited signs of fouling in various degrees. The least colonization of organism was observed from the protected glass substrate area, which showcased the superior anti-biofouling capability by surface double layer disturbance.

Furthermore, this self-activated anti-biofouling system is fairly scalable, which involves less material and lower cost to provide a complete protection compared to conventional coating strategies. In an ideal system (Figure S9)when a high-performance TENG is used[40], we estimated the size of ship hull area that can be protected as a function of TENG size (Figure S10A). For example, for a cruise ship with a length of 184.6 m, only a 75 cm × 60 cm sized TENG would needed to protect the entire underwater area (Figure S10B). One possible strategy to apply the TENG-generated electric field to the entire ship hull is to design an array of interdigitated electrode underneath the regular ship paint (Figure S11), which minimizes the material usage and post-installation care, and we demonstrated applicability

of this design on a board (Figure S12). Another concern for practical application is from the long-term efficiency of the electrical potential generation component, which might be fouled and reduce the performance. First, the TENG surface could be protected by the same strategy. In addition, formation of seriously fouled surface on the TENG would not induce significant influence to the voltage outputs and its antifouling performance (Figure S8).

4. Conclusion

In summary, an efficient and eco-friendly anti-biofouling system was developed using an alternating low-intensity and discrete electric field generated by a water-driven TENG. The anti-biofouling mechanism was attributed to the electric field-induced disturbance to the double layer, which impairs the stable adsorption of organic substances and the subsequent microbe attachments. Systematic analyses confirmed that the anti-biofouling efficacy was directly related to the strength of the electric field. This TENG-driven anti-biofouling could remain active deep into the water as long as the electric field held an appropriate strength. Higher alternating frequency would be favorable particularly for low electric fields; while it would not show much enhancement when the electric field was high, making this strategy very appropriate for low frequency water wave conditions. An on-site demonstration was implemented at a calm lake shore for three weeks. The water-wave driven anti-biofouling exhibited excellent surface protection, which was significantly superior to copper based surfaces and commercial coatings. This development brings a new solution to the long-standing challenge of biofouling in marine systems. It holds a great promise for protecting a broad range of surfaces against biofouling, such as ship's hulls, underwater pipes, oceanographic sensors, drilling equipment, oil platforms, power plants and maybe even medical devices.

Supplementary Material

Refer to Web version on PubMed Central for supplementary material.

Acknowledgements

References

1. Copisarow M, Marine fouling and its prevention. Science 1945, 101, 406–407. [PubMed: 17758725]

2. Fusetani N, Biofouling and antifouling. Nat. Prod. Rep 2004, 21, 94–104. [PubMed: 15039837]

3. Callow JA; Callow ME, Trends in the development of environmentally friendly fouling-resistant marine coatings. Nature communications 2011, 2, 244.

4. Callow ME; Callow JA, Marine biofouling: a sticky problem. Biologist 2002, 49, 1–5.

5. Schultz M; Bendick J; Holm E; Hertel W, Economic impact of biofouling on a naval surface ship. Biofouling 2011, 27, 87–98. [PubMed: 21161774]

6. Braithwaite R; McEvoy L, Marine biofouling on fish farms and its remediation. Adv. Mar. Biol 2005, 47, 215–252. [PubMed: 15596168]

7. Nebot E; Casanueva J; Solera R; Pendon C; Taracido L; Casanueva-Robles T; Lopez-Galindo C, Marine biofouling in heat exchangers. *Biofouling: types, impact and anti-fouling.* New York (NY): Nova Science 2010, 65–104.

8. Jain A; Bhosle NB, Biochemical composition of the marine conditioning film: implications for bacterial adhesion. Biofouling 2009, 25, 13–19. [PubMed: 18846459]

9. Redfield A; Hutchins L; Deevy E; Ayers J; Turner H; Laidlaw F; Ferry J; Todd D, Marine fouling and its prevention US Naval Inst, Annapolis, Md 1952.

10. Compere C; Bellon-Fontaine MN; Bertrand P; Costa D; Marcus P; Poleunis C; Pradier CM; Rondot B; Walls M, Kinetics of conditioning layer formation on stainless steel immersed in seawater. Biofouling 2001, 17, 129–145.

11. Liu Y; Mi B, Effects of organic macromolecular conditioning on gypsum scaling of forward osmosis membranes. J. Membr. Sci 2014, 450, 153–161.

12. Whitehead K; Verran J, The effect of substratum properties on the survival of attached microorganisms on inert surfaces. Marine and industrial biofouling 2009, 13–33. [PubMed: 18846459]

13. Alswieleh AM; Cheng N; Canton I; Ustbas B; Xue X; Ladmiral V; Xia S; Ducker RE; El Zubir O; Cartron ML, Zwitterionic Poly (amino acid methacrylate) Brushes. J. Am. Chem. Soc 2014, 136, 9404–9413. [PubMed: 24884533]

14. Chen K; Zhou S; Wu L, Self-healing underwater superoleophobic and antibiofouling coatings based on the assembly of hierarchical microgel spheres 2015.

15. Ma W; Soroush A; Luong TVA; Brennan G; Rahaman MS; Asadishad B; Tufenkji N, Spray-and spin-assisted layer-by-layer assembly of copper nanoparticles on thin-film composite reverse osmosis membrane for biofouling mitigation. Water Res 2016, 99, 188–199. [PubMed: 27161885]

16. Rasool K; Helal M; Ali A; Ren CE; Gogotsi Y; Mahmoud KA, Antibacterial Activity of Ti3C2T x MXene. ACS nano 2016, 10, 3674–3684. [PubMed: 26909865]

17. Sarvothaman MK; Kim KS; Seale B; Brodersen PM; Walker GC; Wheeler AR, Dynamic Fluoroalkyl Polyethylene Glycol Co-Polymers: A New Strategy for Reducing Protein Adhesion in Lab-on-a-Chip Devices. Adv. Funct. Mater 2015, 25, 506–515.

18. Tesler AB; Kim P; Kolle S; Howell C; Ahanotu O; Aizenberg J, Extremely durable biofouling-resistant metallic surfaces based on electrodeposited nanoporous tungstite films on steel. Nature communications 2015, 6, 8649.

19. Yang R; Jang H; Stocker R; Gleason KK, Synergistic Prevention of Biofouling in Seawater Desalination by Zwitterionic Surfaces and Low-Level Chlorination. Adv. Mater 2014, 26, 1711–1718. [PubMed: 24375685]

20. Liu C; Kong D; Hsu PC; Yuan H; Lee HW; Liu Y; Wang H; Wang S; Yan K; Lin D; Maraccini PA; Parker KM; Boehm AB; Cui Y, Rapid water disinfection using vertically aligned MoS2 nanofilms and visible light. Nat Nanotechnol 2016, 11, 1098–1104. [PubMed: 27525474]

21. Debiemme-Chouvy C; Hua Y; Hui F; Duval J-L; Cachet H, Electrochemical treatments using tin oxide anode to prevent biofouling. Electrochim. Acta 2011, 56, 10364–10370.

22. Wilson RE; Stoianov I; O'Hare D, Biofouling and in situ electrochemical cleaning of a boron-doped diamond free chlorine sensor. Electrochem. Commun 2016, 71, 79–83.

23. Brant KM; Gilg MR, Testing the relative effectiveness of traditional and non-traditional antifouling substrates on barnacle and macroalgae settlement. Mar. Biol. Res 2014, 10, 1027–1032.

24. Woods CM; Floerl O; Jones L, Biosecurity risks associated with in-water and shore-based marine vessel hull cleaning operations. Mar. Pollut. Bull 2012, 64, 1392–1401. [PubMed: 22607846]

25. Schoenbach KH; Joshi RP; Stark RH; Dobbs F; Beebe SJ, Bacterial decontamination of liquids with pulsed electric fields. IEEE Transactions on Dielectrics and Electrical Insulation 2000, 7, 637–645.

26. Hawari AH; Du F; Baune M; Thöming J, A fouling suppression system in submerged membrane bioreactors using dielectrophoretic forces. Journal of Environmental Sciences 2015, 29, 139–145.

27. Zhu G; Su Y; Bai P; Chen J; Jing Q; Yang W; Wang ZL, Harvesting water wave energy by asymmetric screening of electrostatic charges on a nanostructured hydrophobic thin-film surface. ACS nano 2014, 8, 6031–6037. [PubMed: 24745893]

28. Wang X; Niu S; Yin Y; Yi F; You Z; Wang ZL, Triboelectric Nanogenerator Based on Fully Enclosed Rolling Spherical Structure for Harvesting Low-Frequency Water Wave Energy. Advanced Energy Materials 2015, 5.

29. Chen J; Yang J; Li Z; Fan X; Zi Y; Jing Q; Guo H; Wen Z; Pradel KC; Niu S, Networks of triboelectric nanogenerators for harvesting water wave energy: a potential approach toward blue energy. ACS nano 2015, 9, 3324–3331. [PubMed: 25719956]

30. Wen Z; Guo H; Zi Y; Yeh M-H; Wang X; Deng J; Wang J; Li S; Hu C; Zhu L, Harvesting broad frequency band blue energy by a triboelectric–electromagnetic hybrid nanogenerator. ACS nano 2016, 10, 6526–6534. [PubMed: 27267558]

31. Lin ZH; Cheng G; Lee S; Pradel KC; Wang ZL, Harvesting Water Drop Energy by a Sequential Contact-Electrification and Electrostatic-Induction Process. Adv. Mater 2014, 26, 4690–4696. [PubMed: 24830874]

32. Jiang Q; Han Y; Tang W; Zhu H; Gao C; Chen S; Willander M; Cao X; Wang ZL, Self-powered seawater desalination and electrolysis using flowing kinetic energy. Nano Energy 2015, 15, 266–274.

33. Zhao XJ; Tian JJ; Kuang SY; Ouyang H; Yan L; Wang ZL; Li Z; Zhu G, Biocide-Free Antifouling on Insulating Surface by Wave-Driven Triboelectrification-Induced Potential Oscillation. Advanced Materials Interfaces 2016, 3.

34. Xu X-HN; Yeung ES, Long-range electrostatic trapping of single-protein molecules at a liquid-solid interface. Science 1998, 281, 1650–1653. [PubMed: 9733506]

35. Ferrando Chavez DL; Nejidat A; Herzberg M, Viscoelastic Properties of Extracellular Polymeric Substances Can Strongly Affect Their Washing Efficiency from Reverse Osmosis Membranes. Environ. Sci. Technol 2016, 50, 9206–9213. [PubMed: 27404109]

36. Lutskiy M-Y; Avneri-Katz S; Zhu N; Itsko M; Ronen Z; Arnusch CJ; Kasher R, A microbiology-based assay for quantification of bacterial early stage biofilm formation on reverse-osmosis and nanofiltration membranes. Sep. Purif. Technol 2015, 141, 214–220.

37. Herzberg M; Kang S; Elimelech M, Role of extracellular polymeric substances (EPS) in biofouling of reverse osmosis membranes. Environ. Sci. Technol 2009, 43, 4393–4398. [PubMed: 19603652]

38. Geng Z; Zhang H; Xiong Q; Zhang Y; Zhao H; Wang G, A fluorescent chitosan hydrogel detection platform for the sensitive and selective determination of trace mercury (II) in water. Journal of Materials Chemistry A 2015, 3, 19455–19460.

39. Eng J Jr; Hubner I; Barriocanal J; Opila R; Doren D, X-ray photoelectron spectroscopy of nitromethane adsorption products on Si (100): a model for N 1s core-level shifts in silicon oxynitride films. J. Appl. Phys 2004, 95, 1963–1968.

40. Zhu G; Lin Z-H; Jing Q; Bai P; Pan C; Yang Y; Zhou Y; Wang ZL, Toward large-scale energy harvesting by a nanoparticle-enhanced triboelectric nanogenerator. Nano Lett 2013, 13, 847–853. [PubMed: 23360548]
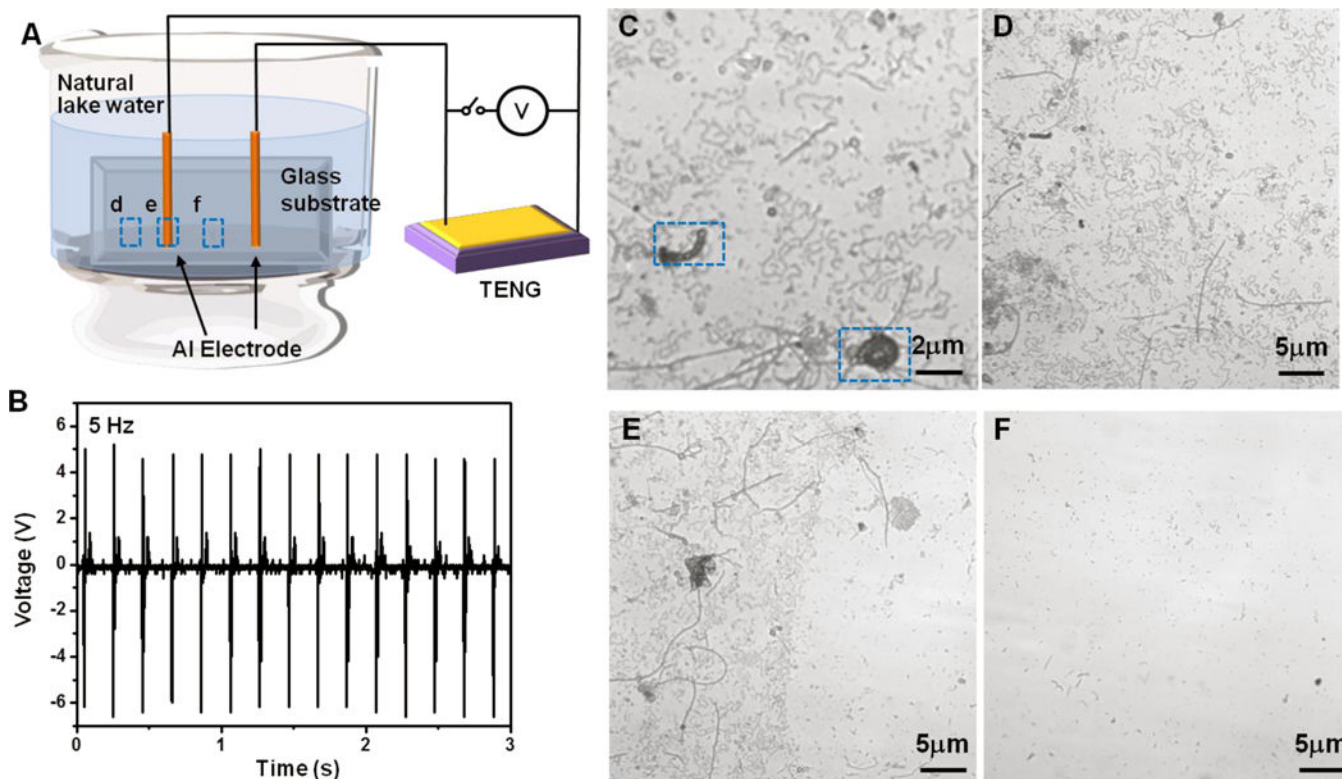
Figure. 1. Anti-biofouling setup and proof-of-concept test.
(A), Schematic setup of the anti-biofouling experiment activated by small and low-frequency electrical pulses produced by a TENG. **(B),** Voltage output profile measured from the TENG, which was used for the anti-biofouling test. **(C),** Microscopic image of small microbes on an unprotected glass surface showing the initiation of biofouling. **(D-F),** Microscopic images of the unprotected area **(D),** the electrode location **(E),** and the protected area **(F),** which are marked in **(A)** accordingly.
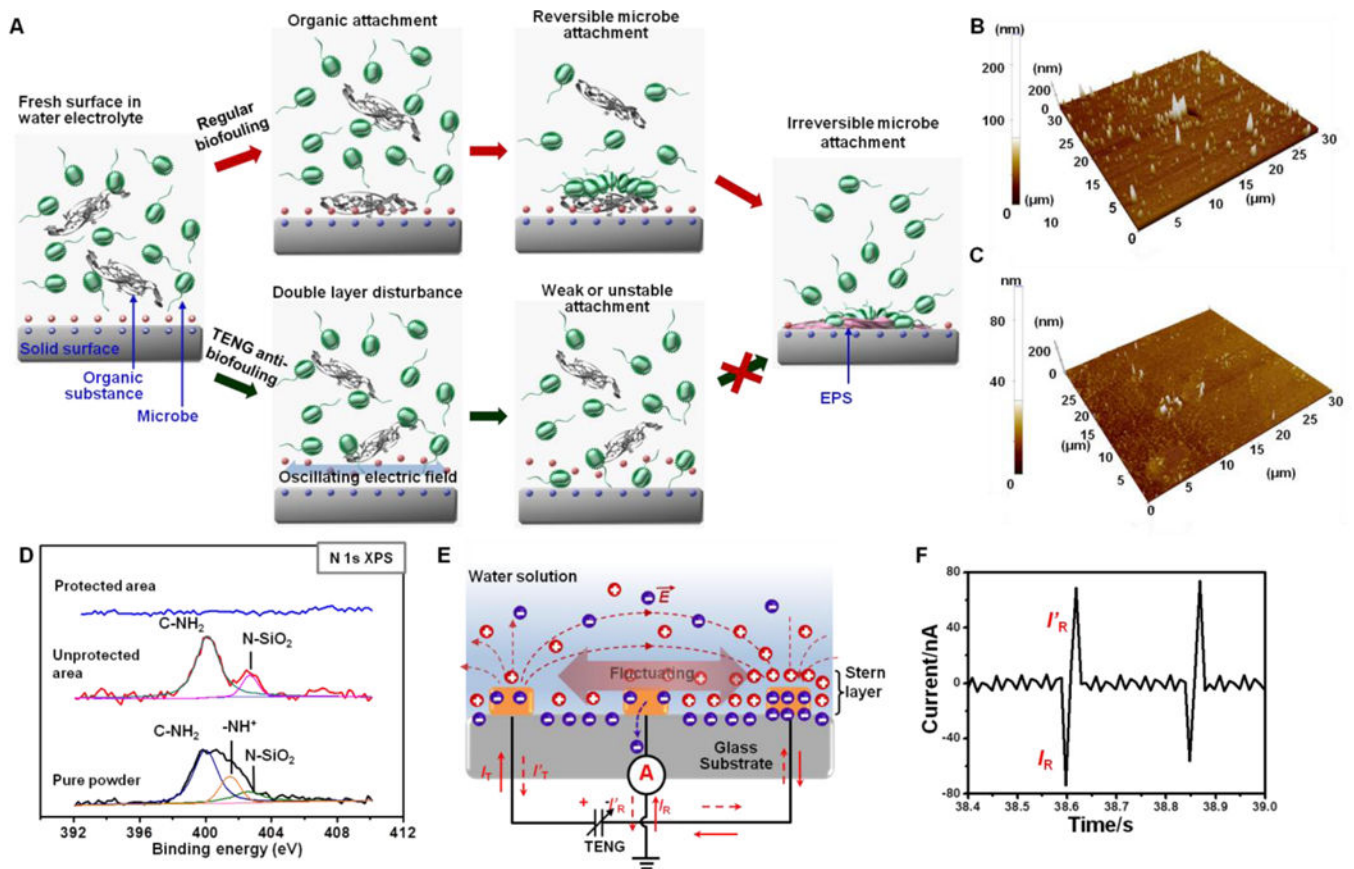
Figure. 2. Mechanism of TENG-driven anti-biofouling.
(A), Schematic of proposed anti-biofouling mechanism. The top route presents a regular biofouling initiation stage from a fresh surface to irreversible microbe attachment. The bottom route illustrates the case where an oscillating electric field exists, the surface double layer was disturbed leading to unstable organic and microbe attachment. **(B,C),** AFM topographic image of unprotected **(B)** and protected **(C)** area after being immersed in a nutrient solution for 1 h. **(D),** XPS spectra compares the surface elemental information of the protected area (blue), unprotected area (red), and the nutrient power (black). **(E),** Schematic illustration of surface charge fluctuation under oscillating electric field generated by TENG. **(F),** Current signal measured between the center reference electrode and group showing a good correlation with TENG output.
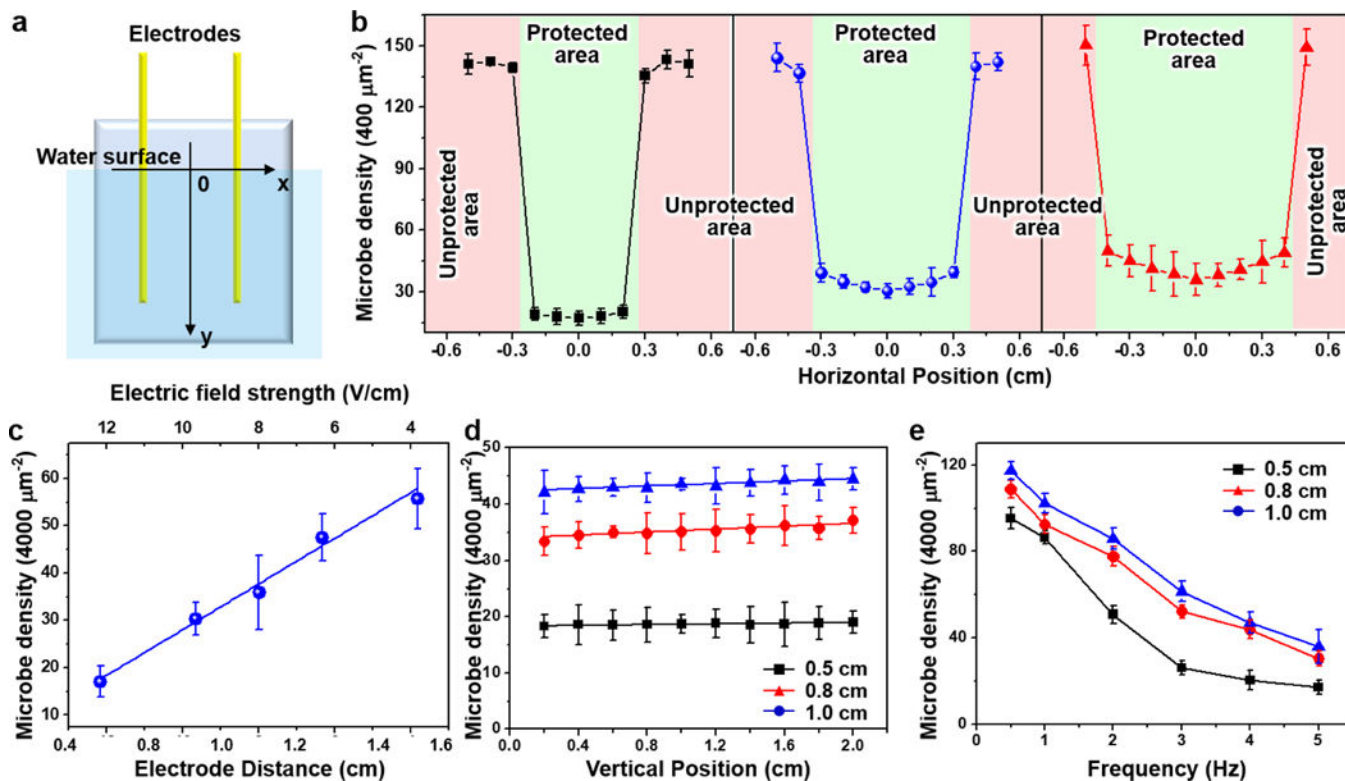
Figure. 3. TENG-driven anti-biofouling performance evaluation.
(A), Schematic diagram of the testing glass geometry. **(B),** Microbe density measured as a function of the horizontal positions (the x direction) for 0.5 cm (black), 0.8 cm (red) and 1.0 cm (blue) electrode distances. **(C),** Microbe density measured at the center position (x=0) as a functional of electrode distance, which is corresponding to the electric field strength (top axis). **(D),** Microbe density measured as a function of the depth beneath the water surface (the y direction) for 0.5 cm (black), 0.8 cm (red) and 1.0 cm (blue) electrode distances. **(E),** Microbe density as a function of the electric field oscillation frequency for 0.5 cm (black), 0.8 cm (red) and 1.0 cm (blue) electrode distances.
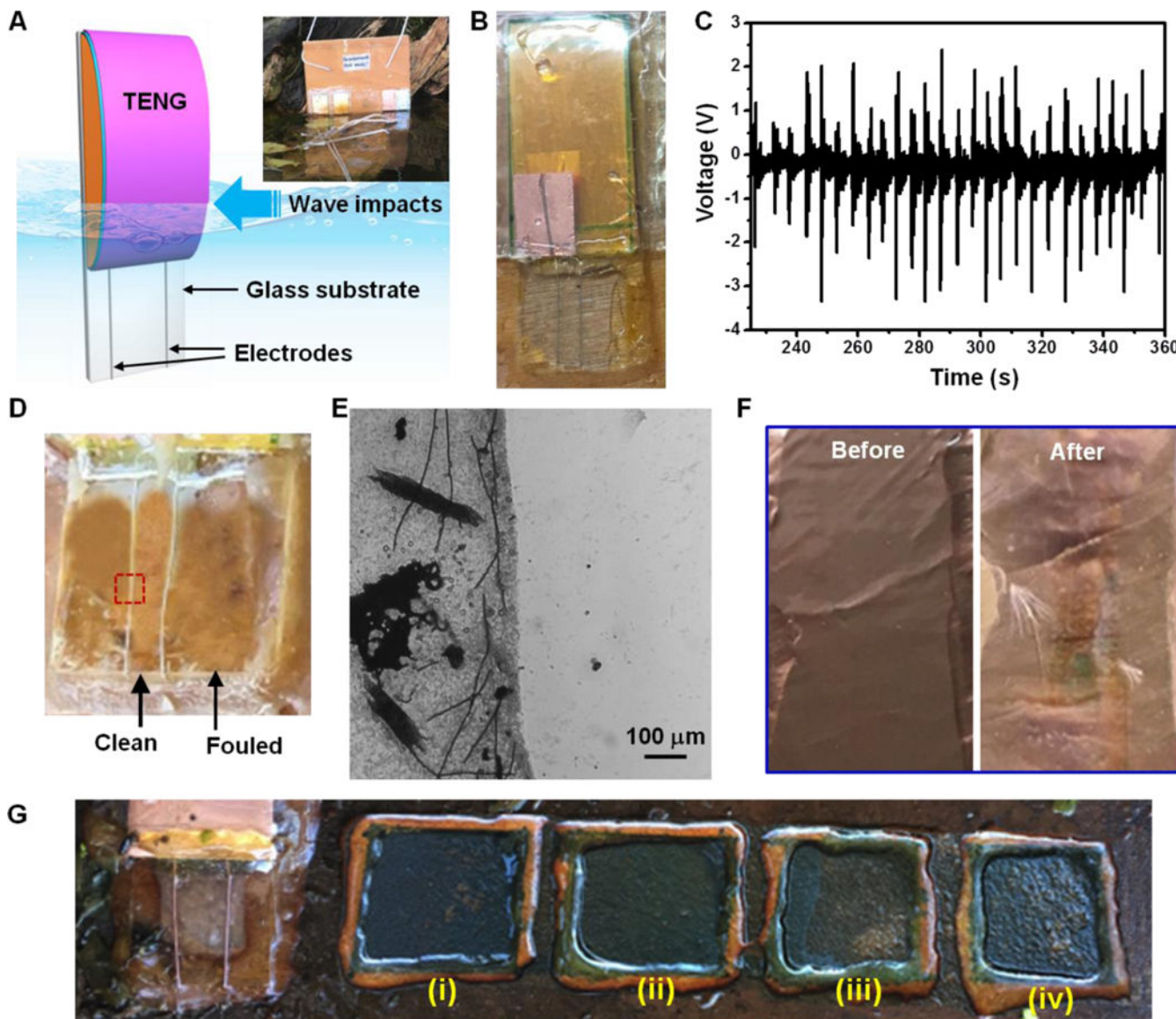
Figure. 4. On-site test of water-driven anti-biofouling.
(A), Schematic of an on-site demonstration setup. Inset shows the water-driven anti-biofouling system and control samples being placed at the shore of lake Mendota. **(B),** A picture of the water-driven anti-biofouling system. **(C),** Voltage output measured from the TENG component under regular water wave impacts. **(D),** The glass surface from the water-driven anti-biofouling system after being placed on-site for 3 weeks. The fouled and protected areas could be clearly distinguished. **(E),** Microscopic image of the glass surface at the electrode wire location showing a distinct boundary. **(F),** Copper surface as a control before and after the 3-week on-site test showing an obvious biofouling feature. **(G),** Comparison of the water-driven anti-biofouling with four commercial anti-fouling coating for 4 weeks of on-site testing, where (i) to (iv) were coatings of Hard hybrid ablative

antifouling, Aerosol antifouling paint, Marine grade aquagard paint, and Aluminipaint, respectivel